JOURNAL OF AIRCRAFT
Vol. 34, No. 3, May–June 1997

Modal-Based Structural Optimization with Static Aeroelastic and Stress Constraints

M. Karpel* and B. Moulin†
Technion—Israel Institute of Technology, Haifa 32000, Israel
and
M. H. Love‡
Lockheed Martin Corporation, Fort Worth, Texas 76101

The modal-based aeroelastic optimization approach is reformulated and extended such that it can deal with more structural analysis and optimization features. The disciplines treated in this paper are statics under fixed loads and static aeroelasticity of free-free aircraft. The new formulation includes the application of stress constraints under fixed and varied external loads, and the effects of inertial changes on aeroelastic trim. It also facilitates the integration of the modal-based option in common finite element structural optimization schemes. The new scheme is applied to realistic design cases using the multidisciplinary automated structural optimization system ASTROS code. Application cases of 3761 and 26,259 degrees of freedom exhibit CPU time reduction factors of 4–122 in comparison with the conventional discrete approach.

Introduction

THE increasing interest in recent years in multidisciplinary design optimization led to the development of several integrated structural optimization schemes for aerospace structures.[1–5] While the dynamic response and stability features are treated in these schemes by the modal approach,[6] the static aeroelastic and stress disciplines are treated by the discrete approach. The application of these design schemes with finite element models of modern flight vehicles, which may include tens of thousands degrees of freedom (DOFs), may be very inefficient or even totally impractical.

The desire for more efficient procedures motivated the development of a reduced-size optimization scheme where calculations of all of the static and dynamic disciplines are based on the modal approach. A single set of low-frequency vibration modes of a baseline structure serves as generalized coordinates. The stability and response parameters of the structure and their sensitivity to changes in the design variables are calculated with respect to these coordinates. The modal approach is especially attractive in multidisciplinary cases where the excitation loads are affected by the structural response, such as in aeroelastic and control-augmented systems. In these repetitive cases, the computation time heavily depends on the number of structural DOFs, which can be reduced with the modal approach by several orders of magnitude.

The applications of modal coordinates for calculating static aeroelastic effectiveness parameters[7,8] and external loads,[9] and their derivatives with respect to design variables, were shown in Refs. 7 and 8 to be very efficient and accurate. Modal-based multidisciplinary optimization with aeroelastic effectiveness, flutter, and control stability margins was presented in Ref. 10. The modal approach was extended in Ref. 11 to deal with static optimization disciplines with stress constraints. Applications to an 800-DOF model of a transport aircraft with a high-aspect-ratio wing showed excellent results for pull-up maneuver cases analyzed with 20–40 baseline modes.

The main reason for not using the modal approach in stress analysis is that it might yield erroneous results in cases of concentrated loads and in cases of large local structural changes. Recent developments of the modal approach facilitated the application of practical techniques to overcome these difficulties with minimal impact on the efficiency of the modal approach. Fictitious masses,[12] which are added to the structure when the baseline modal coordinates are defined, can be used to deal with local excitation[13] and with large local stiffness changes.[14] Modal perturbations[11] can be used to yield high-accuracy stresses in modal-based structural optimization. The method of Ref. 11 was applied in a simple aeroelastic optimization scheme that did not address all of the options and capabilities needed for advanced industrial applications.

The purposes of the work presented in this paper were the modification and extension of the modal-based formulation such that it can deal with more general analysis and optimization cases, its application in the automated structural optimization system (ASTROS),[2] and its demonstration with realistic design cases.

Generalized Structural Matrices

The structural stiffness and mass matrices in common finite element codes are first assembled with respect to all of the structural discrete DOFs. The application of single and multipoint constraints eliminates the dependent coordinates and generates the free-coordinate matrices $[K_{ff}]$ and $[M_{ff}]$. A further common optional reduction of the number of DOFs is Guyan's static condensation method.[15] The resulting stiffness and mass matrices, $[K_{aa}]$ and $[M_{aa}]$, are used in the basic structural equilibrium analysis. The formulation shown later in this paper assumes that if static condensation is applied, it involves only structural parts that are not changed in the optimization process.

The gauges of selected elements of the model serve as design variables in the optimization process. A global design variable is a changeable factor that multiplies the stiffness and mass matrices of a user-defined group of finite elements. To accommodate changes in the n_{dv} global design variables, the

Presented as Paper 96-1479 at the AIAA/ASME/ASCE/AHS/ASC 37th Structures, Structural Dynamics, and Materials Conference, Salt Lake City, UT, April 15–17, 1996; received May 23, 1996; revision received Jan. 21, 1997; accepted for publication Jan. 24, 1997.

*Associate Professor, Faculty of Aerospace Engineering. Member AIAA.
†Research Associate, Faculty of Aerospace Engineering.
‡Engineering Specialist Senior, Technology Integration. Senior Member AIAA.

matrices are assembled in the design loop by adding the contribution of the design changes to the contribution of the baseline (initial) model. It is assumed in this paper that the structural matrices are linear with respect to the design variables, namely

$$[K_{aa}] = [K_{aa}]_b + \sum_{i=1}^{n_{dv}} (v_i - v_{b_i}) \frac{\partial [K_{aa}]}{\partial v_i} \tag{1}$$

$$[M_{aa}] = [M_{aa}]_b + \sum_{i=1}^{n_{dv}} (v_i - v_{b_i}) \frac{\partial [M_{aa}]}{\partial v_i} \tag{2}$$

where v_i is the current value of the ith design variable and the subscript b relates to the baseline structure. The assumption of linearity in Eqs. (1) and (2) simplifies the subsequent formulation, but is not vital. Additional terms, such as cubic terms for out-of-plane bending of plates and noninteger powers of v_i for bar elements,[16] can be handled in a similar manner.

The regular discrete approach assembles the global matrices and reduces them to the analysis set in each optimization iteration. The modal approach does it only once, for the baseline design. The analysis matrices $[K_{aa}]_b$ and $[M_{aa}]_b$ are used to calculate a set of low-frequency vibration modes $[\phi_a]$, with n_r rigid-body modes and n_e elastic ones, which serve as generalized coordinates in subsequent analyses. For consistency with the regular ASTROS formulation, the rigid-body modes $[\phi_{ar}]$ are replaced by rigid translations and rotations with respect to user-defined reference grid point

$$[\bar{\phi}_{ar}] \equiv \begin{bmatrix} \bar{\phi}_{lr} \\ \bar{\phi}_{rr} \end{bmatrix} = \begin{bmatrix} D \\ I \end{bmatrix} \tag{3}$$

where $[D]$ is a rigid-body transformation matrix. The resulting rigid-body mass matrix is a full matrix:

$$[M_{rr}]_b = [\bar{\phi}_{ar}]^T [M_{aa}]_b [\bar{\phi}_{ar}] \tag{4}$$

Because of mode orthogonality, the baseline mass coupling $[M_{er}]_b$ between the rigid-body and elastic modes equals zero. The stiffness associated with the rigid-body modes is zero. The baseline generalized stiffness matrix associated with the elastic modes is a positive-definite diagonal matrix:

$$[K_{ee}]_b = [\phi_{ae}]^T [K_{aa}]_b [\phi_{ae}] \tag{5}$$

The basic assumption of the modal approach in structural optimization is that the structural displacements (static or dynamic) in response to external excitation can be adequately expressed as a linear combination of the baseline modes

$$\{u_a\} = [\bar{\phi}_{ar}]\{\xi_r\} + [\phi_{ae}]\{\xi_e\} \tag{6}$$

where $\{u_a\}$ is the analysis-set structural displacement vector, and $\{\xi_r\}$ and $\{\xi_e\}$ are vectors of rigid and elastic generalized (modal) displacements, respectively.

The pre- and postmultiplication of Eqs. (1) and (2) by the mode-shape matrices yield expressions for the updated generalized stiffness and mass matrices

$$[K_{ee}] = [K_{ee}]_b + \sum_{i=1}^{n_{dv}} (v_i - v_{b_i}) \frac{\partial [K_{ee}]}{\partial v_i} \tag{7}$$

$$\begin{bmatrix} M_{rr} \\ M_{er} \end{bmatrix} = \begin{bmatrix} M_{rr} \\ 0 \end{bmatrix}_b + \sum_{i=1}^{n_{dv}} (v_i - v_{b_i}) \frac{\partial}{\partial v_i} \begin{bmatrix} M_{rr} \\ M_{er} \end{bmatrix} \tag{8}$$

where the contributions of the global design variables to the generalized stiffness and mass matrices are

$$\frac{\partial [K_{ee}]}{\partial v_i} = [\phi_{ae}]^T \frac{\partial [K_{aa}]}{\partial v_i} [\phi_{ae}] \tag{9}$$

$$\frac{\partial}{\partial v_i} \begin{bmatrix} M_{rr} \\ M_{er} \end{bmatrix} = [\bar{\phi}_{gr} \quad \phi_{ae}]^T \frac{\partial [M_{aa}]}{\partial v_i} [\bar{\phi}_{ar}] \tag{10}$$

These matrices are calculated for the baseline structure and stored in the database before the optimization starts.

Static Analysis Under Fixed Loads

The modal formulation of Ref. 11 was developed for the consideration of stress constraints in aeroelastic optimization. To facilitate the integration of the modal approach in common structural analysis and design schemes the formulation is first modified to deal with fixed external loads, when the net loads (the sum of external and inertial loads) are changed when the structure is free, because of changeable inertia relief effects. The full aeroelastic problem is discussed in the subsequent sections. We also make the procedure more general by separating the analysis of the baseline structure and that of the modified structure.

The equilibrium equation for discrete-coordinate static analysis of a free-free structure is

$$[K_{aa}]\{u_a\} + [M_{aa}]\{\ddot{u}_a\} = \{P_a\} \tag{11}$$

where $\{P_a\}$ is the vector of fixed external loads. The substitution of the modal assumption, Eq. (6), and the premultiplication $[\bar{\phi}_{ar} \quad \phi_{ae}]^T$ yields

$$\begin{bmatrix} 0 \\ K_{ee} \end{bmatrix} \{\xi_e\} + \begin{bmatrix} M_{rr} \\ M_{er} \end{bmatrix} \{\ddot{\xi}_r\} = \begin{bmatrix} \bar{\phi}_{ar}^T \\ \phi_{ae}^T \end{bmatrix} \{P_a\} \tag{12}$$

where the effects of $\{\ddot{\xi}_e\}$ are neglected. The first row in Eq. (12) can be solved for the rigid-body accelerations

$$\{\ddot{\xi}_r\} = [M_{rr}]^{-1} [\bar{\phi}_{ar}]^T \{P_a\} \tag{13}$$

The second row of Eq. (12) can then be solved for the elastic modal deformations

$$\{\xi_e\} = [K_{ee}]^{-1} ([\phi_{ae}]^T \{P_a\} - [M_{er}]\{\ddot{\xi}_r\}) \tag{14}$$

Equation (13) vanishes, of course, when the structure is clamped in all directions such that $\{\xi_r\}$ is empty. The second term of Eq. (14) reflects only secondary inertia relief effects in the free-free case. The primary effects are applied implicitly because the elastic modes are orthogonal to the rigid-body ones, with respect to the baseline mass matrix.

Response of Baseline Structure

The baseline structural displacements can be recovered from $\{\xi_e\}$ by the elastic part of Eq. (6). However, for consistency with the static analysis part of ASTROS, the elastic modes are shifted by rigid-body displacements such that the displacements at the reference point are $\{u_r\} = 0$. The other displacements, which form the l partition of $\{u_a\}$, become

$$\{u_l\}_b = [\bar{\phi}_{le}]\{\xi_e\}_b \tag{15}$$

where

$$[\bar{\phi}_{le}] = [\phi_{le}] - [D][\phi_{re}]$$

where $[\phi_{re}]$ and $[\phi_{le}]$ are the r and l row partitions of $[\phi_{ae}]$. The displacements of Eq. (15) can be used to calculate element stresses for the baseline structure.

Response of Modified Structure

The relatively simple examples of Ref. 11 demonstrated an excellent agreement between the baseline stresses calculated by the modal-approach displacements, Eq. (15), and those of the discrete approach. However, when the baseline modes were used to calculate stresses of the modified structure, additional information was required.

The displacement vector for stress analysis of the modified structure is composed by

$$\{\boldsymbol{u}_l\} = \{\boldsymbol{u}_l\}_0 + \{\boldsymbol{\Delta u}\} \tag{16}$$

where $\{\boldsymbol{u}_l\}_0$ is the elastic displacement of the baseline structure under the modified net loads, and $\{\boldsymbol{\Delta u}\}$ is the change of the displacements because of the change in stiffness. While the first term in Eq. (16) can still be calculated by the regular modal approach of Eq. (15), with $\{\xi_e\}_b$ replaced by the hypothetical $\{\xi_e\}_0$, the second term requires modal perturbations.

Unlike for stresses in the modified structure, net loads can be adequately based on the mode-displacement assumption.[11] It should be noted that, even though the external loads are fixed in this section, the net loads change with the mass of the design variables. With the modal approximation of Eq. (6), the modified net-load vector is approximated by

$$\{\boldsymbol{F}_a\} = [K_{aa}][\phi_{ae}]\{\xi_e\} \tag{17}$$

Premultiplication by $[\phi_{ae}]^T$ and application to the baseline structure gives the equilibrium equation for the hypothetical generalized displacements

$$[K_{ee}]_b\{\xi_e\}_0 = [K_{ee}]\{\xi_e\} \tag{18}$$

The extraction of $\{\xi_e\}_0$ and its substitution in for $\{\xi_e\}_b$ in Eq. (15), using Eq. (7) for $[K_{ee}]$, yields

$$\{\boldsymbol{u}_l\}_0 = [\bar{\phi}_{le}]\left([I] + \sum_{i=1}^{n_{dv}} (v_i - v_{b_i})[K_{ee}]_b^{-1}\frac{\partial[K_{ee}]}{\partial v_i}\right)\{\xi_e\} \tag{19}$$

The second term in Eq. (16) represents the displacement changes because of forces applied by the added material on the baseline structure. Because of the local nature of these internal loads, this term cannot be adequately based on the regular modal assumption.[11] To avoid the costly reconstruction and solution of the full finite element equilibrium equation in each optimization step, $\{\boldsymbol{\Delta u}\}$ is approximated by

$$\{\boldsymbol{\Delta u}\} = \left[\sum_{i=1}^{n_{dv}} (v_i - v_{b_i})[\phi_{FI}]_i\right]\{\xi_e\} \tag{20}$$

where $[\phi_{FI}]_i$ are modal perturbation matrices that reflect local deformations that are added to database modes because of unit change of the ith design variable. These perturbations are based on static response modes calculated for the baseline structure before the optimization starts by solving the discrete-coordinate equation

$$[K_{II}]_b[\phi_{FI}]_i = [\bar{F}_I]_i \tag{21}$$

where $[K_{II}]_b$ is the baseline $[K_{aa}]$ after eliminations of the rows and columns associated with the reference r degrees of freedom, and $[\bar{F}_I]_i$ is the l row partition of

$$[\bar{F}_a]_i = -\frac{\partial[K_{aa}]}{\partial v_i}[\phi_{ae}] \tag{22}$$

Equations (16), (19), and (20) yield

$$\{\boldsymbol{u}_l\} = [\phi_S]\{\xi_e\} \tag{23}$$

where

$$[\phi_S] = [\bar{\phi}_{le}] + \sum_{i=1}^{n_{dv}} (v_i - v_{b_i})[\phi_{TI}]_i$$

where the modified perturbation matrices

$$[\phi_{TI}]_i = [\phi_{FI}]_i + [\bar{\phi}_{le}][K_{ee}]_b^{-1}\frac{\partial[K_{ee}]}{\partial v_i} \tag{24}$$

are stored in the database for repeated analysis and sensitivity calculations. The calculation of stress and strain constraints from $\{\boldsymbol{u}_l\}$ of Eq. (23) is identical to that of the discrete approach.

It can be observed that, with $v_i = v_{b_i}$, $\{\boldsymbol{u}_l\}$ of Eq. (23) is equal to $\{\boldsymbol{u}_l\}_b$ of Eq. (15), which shows that the modal perturbations are not used for stress and strain analysis of the baseline structure. However, their effect on stress and strain sensitivities starts in the baseline structure.

Sensitivity Analysis with Fixed Loads

The equilibrium modal displacements $\{\xi_e\}$ and rigid-body accelerations $\{\ddot{\xi}_r\}$ (when the structure is free), are used to calculate the sensitivity of the structural displacements to changes in the design variables v_i. The differentiation of Eq. (13) with respect to v_i yields

$$\frac{\partial\{\ddot{\xi}_r\}}{\partial v_i} = -[M_{rr}]^{-1}\frac{\partial[M_{rr}]}{\partial v_i}\{\ddot{\xi}_r\} \tag{25}$$

The differentiation of Eq. (14) yields

$$\frac{\partial\{\xi_e\}}{\partial v_i} = -[K_{ee}]^{-1}\left(\frac{\partial[K_{ee}]}{\partial v_i}\{\xi_e\} + \frac{\partial[M_{er}]}{\partial v_i}\{\ddot{\xi}_r\} + [M_{er}]\frac{\partial\{\ddot{\xi}_r\}}{\partial v_i}\right) \tag{26}$$

The differentiation of Eq. (23) gives

$$\frac{\partial\{\boldsymbol{u}_l\}}{\partial v_i} = [\phi_{TI}]_i\{\xi_e\} + [\phi_S]\frac{\partial\{\xi_e\}}{\partial v_i} \tag{27}$$

which merges with $\partial\{\boldsymbol{u}_r\}/\partial v_i = 0$ to form $\partial\{\boldsymbol{u}_a\}/\partial v_i$. The subsequent calculation of stress and strain sensitivities is straightforward and identical to that of the discrete approach. As will be discussed in the numerical example section, the computational savings of the modal approach in structural optimization under fixed loads are small compared to the savings in static aeroelastic cases, which are based on the same database of modes and modal perturbations.

Static Aeroelastic Analysis

Common aeroelastic analysis and design codes such as MSC/NASTRAN[3] and ASTROS[16] start the aerodynamic part by defining a linear aerodynamic panel model for which a steady aerodynamic influence coefficient matrix and a unit aerodynamic force matrix (because of aerodynamic parameters such as unit angle of attack, pitch rate, or control surface deflection) are generated. Spline interpolation matrices are then used to transform the aerodynamic matrices to the structural grid. The modal approach of this paper uses the baseline modes $[\phi_{ar}]$ and $[\phi_{ae}]$ to transform these matrices to generalized coordinates. The resulting generalized aerodynamic matrices are independent of the design variables.

The static aeroelastic equilibrium equation in generalized coordinates is

$$\begin{bmatrix} -qA_{rr} & -qA_{re} \\ -qA_{er} & K_{ee} - qA_{ee} \end{bmatrix} \begin{Bmatrix} \xi_r \\ \xi_e \end{Bmatrix} + \begin{bmatrix} M_{rr} \\ M_{er} \end{bmatrix} \{\ddot{\xi}_r\} = \begin{bmatrix} P_{r\delta} \\ P_{e\delta} \end{bmatrix} \{\delta\} \quad (28)$$

where the effects of $\{\ddot{\xi}_e\}$ are neglected, q is the dynamic pressure, and $\{\delta\}$ is the vector of trim variables. Another equation is defined by the requirement of orthogonality between the displacement vector $\{u_a\}$ and the rigid-body modes

$$[\bar{\phi}_{ar}]^T [M_{aa}] \{u_a\} = \{0\} \quad (29)$$

The substitution of $\{u_a\}$ from Eq. (6) yields

$$\{\xi_r\} = -[M_{rr}]^{-1} [M_{er}]^T \{\xi_e\} \quad (30)$$

which equals zero for the baseline structure, when $[M_{er}] = 0$. The substitution of Eq. (30) in the second row of Eq. (28) gives

$$\{\xi_e\} = [\bar{K}_{ee}]^{-1} ([P_{e\delta}]\{\delta\} - [M_{er}]\{\ddot{\xi}_r\}) \quad (31)$$

where

$$[\bar{K}_{ee}] = [K_{ee}] - q[A_{ee}] + q[A_{er}][M_{rr}]^{-1}[M_{er}]^T$$

The substitution of Eq. (31) in the first row of Eq. (28) gives

$$[\bar{M}_{rr}]\{\ddot{\xi}_r\} = [\bar{P}_{r\delta}]\{\delta\} \quad (32)$$

where

$$[\bar{M}_{rr}] = [M_{rr}] + q[\bar{A}_{re}][\bar{K}_{ee}]^{-1}[M_{er}]$$

$$[\bar{P}_{r\delta}] = [P_{r\delta}] + q[\bar{A}_{re}][\bar{K}_{ee}]^{-1}[P_{e\delta}]$$

where

$$[\bar{A}_{re}] = [A_{re}] - [A_{rr}][M_{rr}]^{-1}[M_{er}]^T$$

Equation (32) is the basic equation for static aeroelastic analysis. The user defines all of the variables in $\{\ddot{\xi}_r\}$ and $\{\delta\}$, except for n_r free variables that are solved for by Eq. (32). The trim vectors are then used to calculate the modal deflections $\{\xi_e\}$ by Eq. (31) and $\{\xi_r\}$ by Eq. (30). The discrete elastic deflections for stress analysis can now be calculated with Eq. (23), using the same modal perturbations as in the fixed-loads case. Another option is to use Eq. (6) for calculating the structural displacements without modal-perturbation effects, use the aerodynamic matrices described at the beginning of this section to calculate aerodynamic loads, and then resort to the regular discrete-coordinate stress analysis.

When Eq. (32) is applied to the baseline model, $[M_{er}] = 0$ and $[\bar{M}_{rr}] = [M_{rr}]$. The terms of $[\bar{P}_{r\delta}]$ in this case are the flexible aerodynamic forces and moments per unit aerodynamic parameters, whereas those of $[P_{r\delta}]$ of Eq. (28) are the rigid ones. In the more general case, when the model is modified, we can rewrite Eq. (32) as

$$[M_{rr}]\{\ddot{\xi}_r\} = [\tilde{P}_{r\delta}]\{\delta\} \quad (33)$$

where

$$[\tilde{P}_{r\delta}] = [M_{rr}][\bar{M}_{rr}]^{-1}[\bar{P}_{r\delta}]$$

The flex-to-rigid ratios between terms in $[\tilde{P}_{r\delta}]$ and $[P_{r\delta}]$ define the aeroelastic effectiveness parameters which can be used as optimization constraints:

$$\varepsilon_{jk} = \tilde{P}_{r\delta_{jk}} / P_{r\delta_{jk}} \quad (34)$$

Static Aeroelastic Sensitivity Analysis

The differentiation of Eq. (28) with respect to the design variable v_i can be written as

$$\begin{bmatrix} -qA_{rr} & -qA_{re} \\ -qA_{er} & K_{ee} - qA_{ee} \end{bmatrix} \frac{\partial}{\partial v_i} \begin{Bmatrix} \xi_r \\ \xi_e \end{Bmatrix} + \begin{bmatrix} M_{rr} \\ M_{er} \end{bmatrix} \frac{\partial \{\ddot{\xi}_r\}}{\partial v_i} = \begin{bmatrix} P_{r\delta} \\ P_{e\delta} \end{bmatrix} \frac{\partial \{\delta\}}{\partial v_i} - \frac{\partial}{\partial v_i} \begin{bmatrix} 0 & M_{rr} \\ K_{ee} & M_{er} \end{bmatrix} \begin{Bmatrix} \ddot{\xi}_e \\ \ddot{\xi}_r \end{Bmatrix} \quad (35)$$

The differentiation of Eq. (30) yields

$$\frac{\partial \{\xi_r\}}{\partial v_i} = -[M_{rr}]^{-1} \left(\frac{\partial [M_{rr}]}{\partial v_i} \{\xi_r\} + \frac{\partial [M_{er}]^T}{\partial v_i} \{\xi_e\} + [M_{er}]^T \frac{\partial \{\xi_e\}}{\partial v_i} \right) \quad (36)$$

Equations (35) and (36) combine for the trim sensitivity equation

$$[\bar{M}_{rr}] \frac{\partial \{\ddot{\xi}_r\}}{\partial v_i} = [\bar{P}_{r\delta}] \frac{\partial \{\delta\}}{\partial v_i} + \{\Delta \bar{P}_r\}_i \quad (37)$$

where $[\bar{M}_{rr}]$ and $[\bar{P}_{r\delta}]$ are defined in Eq. (32) and

$$\{\Delta \bar{P}_r\}_i = -q(q[\bar{A}_{re}][\bar{K}_{ee}]^{-1}[A_{er}] + [A_{rr}])[M_{rr}]^{-1} \times \left(\frac{\partial [M_{rr}]}{\partial v_i} \{\xi_r\} + \frac{\partial [M_{er}]^T}{\partial v_i} \{\xi_e\} \right) - \frac{\partial [M_{rr}]}{\partial v_i} \{\ddot{\xi}_r\} - q[A_{re}][\bar{K}_{ee}]^{-1} \left(\frac{\partial [GK_{ee}]}{\partial v_i} \{\xi_e\} + \frac{\partial [M_{er}]}{\partial v_i} \{\ddot{\xi}_r\} \right) \quad (38)$$

The truncation of all the columns in $[\bar{M}_{rr}]$ and $[\bar{P}_{r\delta}]$ in Eq. (37) that are associated with the fixed trim variables yields an equation for the n_r derivatives of the free variables. Once these are calculated, the derivatives of $\{\xi_r\}$ are calculated by Eq. (36) and the derivatives of $\{\xi_e\}$ by the second row of Eq. (35). The expression for the derivatives of the displacements for stress and strain analyses is identical to that of the fixed-load case, Eq. (27).

The sensitivity of the aeroelastic effectiveness parameters of Eq. (34) are based on the differentiation of $[\tilde{P}_{r\delta}]$ of Eq. (33), which yields

$$\frac{\partial [\tilde{P}_{r\delta}]}{\partial v_i} = \frac{\partial [M_{rr}]}{\partial v_i} [a_r] + [M_{rr}][\bar{M}_{rr}]^{-1} [\Delta \bar{P}_r]_i \quad (39)$$

where

$$[a_r] = [\bar{M}_{rr}]^{-1} [\bar{P}_{r\delta}]$$

and $[\Delta \bar{P}_r]_i$ is calculated by Eq. (38) with $\{\ddot{\xi}_r\}$ replaced by $[a_r]$, $\{\xi_e\}$ replaced by

$$[X_e] = [\bar{K}_{ee}]^{-1} ([P_e] - [M_{er}][a_r]) \quad (40)$$

and $\{\xi_r\}$ replaced by

$$[X_r] = -[M_{rr}]^{-1} [M_{er}]^T [X_e] \quad (41)$$

Numerical Examples

The purpose of the numerical examples is to demonstrate the accuracy and efficiency of the modal approach, as utilized by modifying the static parts of ASTROS, in comparison with the discrete approach of ASTROS[16] Version 11.0. Two examples are given, optimization for minimum weight under stress constraints of a maneuvering generic fighter aircraft with 3761 DOFs, and aeroelastic trim and effectiveness analysis of an actual fighter aircraft with 26,259 DOFs.

The first example is based on a generic advanced fighter aluminum (AFA) model. A top view of the USSAERO[16] aerodynamic model is given in Fig. 1. The structural model consists of 1276 grid points and 4449 elements, and has 3761 free DOFs. A top view of the skin elements in the wing structural model is shown in Fig. 2. The wing box is divided into 13 zones. The thickness values of the upper and lower skin elements in each zone are multiplied in the optimization process by a common factor, for a total of 26 global design variables. The inner structure of the wing, as well as the structure of the rest of the aircraft, are not subjected to changes.

A single case with symmetric boundary conditions is optimized for a minimum weight of the wing–box skin. Stress constraints are applied for a single symmetric $9g$ pull-up maneuver where the loads are based on aeroelastic trim. The modal optimization was performed with 45 low-frequency elastic modes taken into account. The von Mises stresses σ_i of the wing–box skin elements are constrained to less than $\sigma_{\text{limit}} =$ 36,700 psi. The initial weight of the designed skin is 679 lb. The variation of this weight along the optimization path, for discrete and modal optimization cases, is given in Fig. 3. The initial skin is obviously overdesigned. The discrete optimization process reduces the weight to 526 lb in four iterations. The modal-based process converged after three iterations in this case to a 512-lb design, which implies that the modal-based weight reduction was about 10% more than that of the discrete reduction. A second modal optimization run, which started with the creation of a new database for the final model of the first modal run, converged in two steps to a 528-lb model. Similar trends are shown in Fig. 4, which compares the variations of typical skin thickness values along the optimization paths.

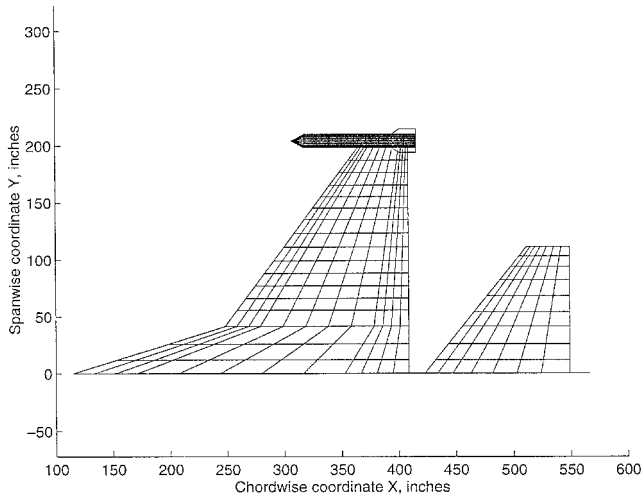

Fig. 1 AFA USSAERO model.

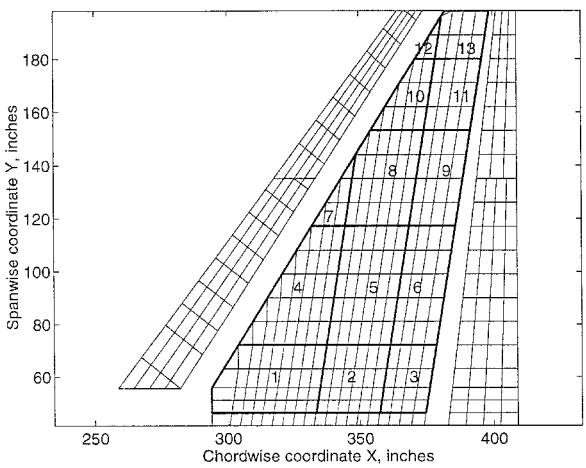

Fig. 2 AFA structural optimization zones.

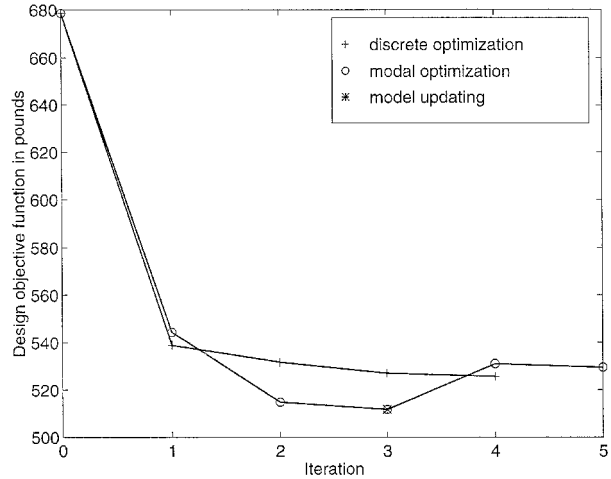

Fig. 3 Weight of the designed skin along the optimization paths.

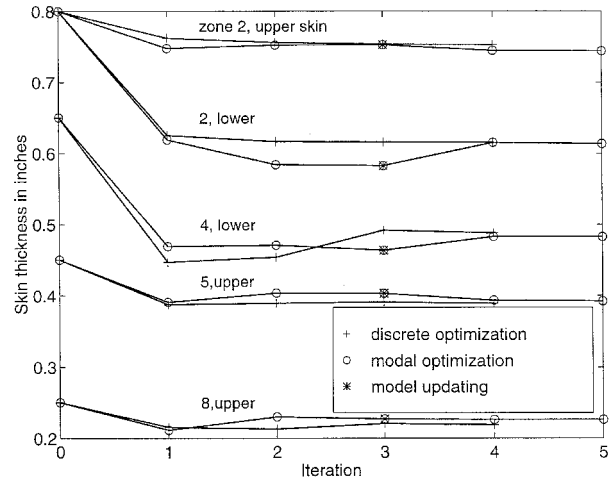

Fig. 4 Typical thickness values along the optimization paths.

The wing stress field along the span of the second row of elements across zones 2, 5, and 8 of Fig. 2 is shown in Fig. 5 for various stages of the optimization runs. The dashed line gives the baseline von Mises stresses, calculated by the standard discrete approach. The calculation of these stresses with the modal approach gave practically identical results (not shown). The full line gives the stress field after the four-step discrete optimization. The stress field at the end of the first (three-step) modal optimization run, based on the baseline modes, is given by the circles. These stresses are in good agreement with those of the discrete optimization (full line). The last case shown in Fig. 5 is the stress field at the end of the first optimization, as calculated with the modes of the updated model (which is the baseline for the second modal optimization run). These stresses are different than those calculated before the mode update (circles) by up to 7.5% over the entire wing. The stresses in the final analysis at the end of the second modal optimization run (not shown) are practically

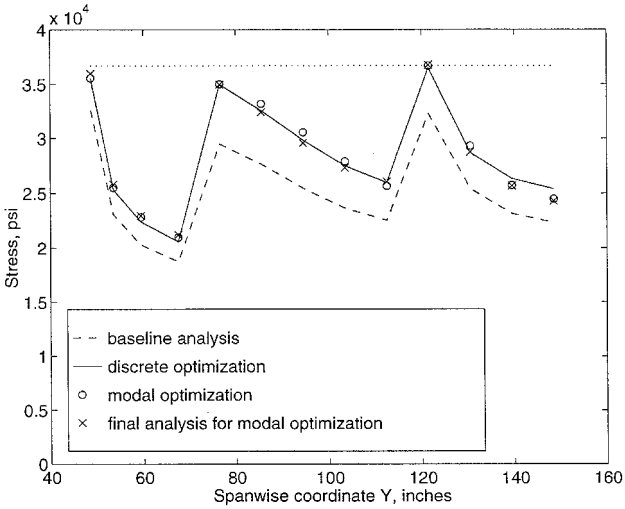

Fig. 5 AFA wing stress field.

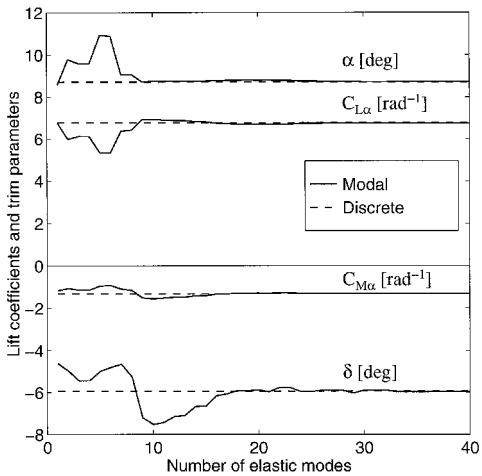

Fig. 6 Aerodynamic coefficients and trim variables for the baseline structure vs number of baseline modes.

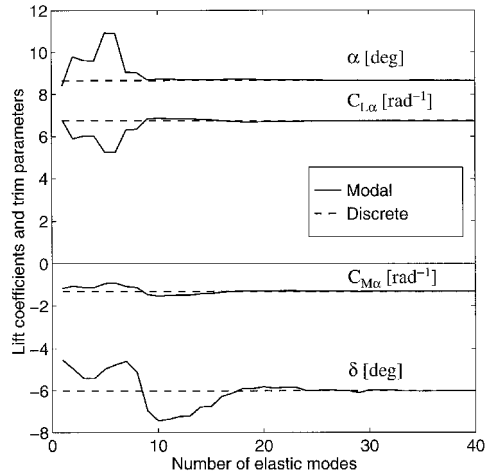

Fig. 7 Aerodynamic coefficients and trim variables for a modified structure vs number of baseline modes.

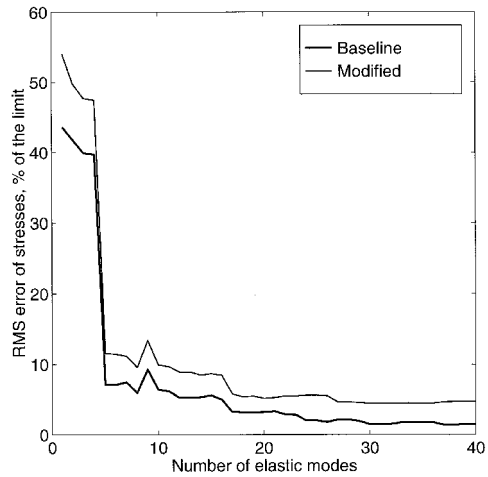

Fig. 8 Root-mean-square wing–box stress errors vs number of baseline modes.

identical to those at the end of the discrete optimization process (full line).

When applied to a baseline structure, the modal approach was always in almost perfect agreement with the discrete approach, in this particular example, for stress and trim parameters and their sensitivities. Changes of about 10% in the design variables without updating the modes lead to modal errors of up to 2% in high stresses and less than 1% in trim variables. The maximum errors grew to 5 and 2%, respectively, with design changes of about 20%, and to 10 and 4% with design changes of 30%. These errors, and the computational efficiency considerations given later in this paper, can be used as guidelines for choosing optimization methodology and design move limits.

To demonstrate the effects of the number of elastic modes taken into account, the first three-step modal optimization run was repeated with the number of elastic modes taken into account varying from 1 to 48. The convergence plots of the trim angle of attack α and elevator deflection δ, and the lift and moment coefficients C_{L_α} and C_{M_α}, are shown in Fig. 6 for the baseline structure and in Fig. 7 for the final one. The respective discrete-analysis coefficients are also shown for comparison in dashed lines. It can be observed that excellent results are obtained in both cases with about 25 modes of the baseline structure. Even with the considerable structural changes, when the weight of the wing–box skin is reduced by 25% (from 679 to 521 lb), the accuracy with any number of modes (Fig. 7) is similar to that of the baseline structure (Fig. 6).

An overall measure for the stress accuracy in the modal approach is the rms value of the differences between the wing–box modal σ_i and the respective discrete stresses, divided by σ_{limit}. The variations of this measure with the number of elastic modes taken into account are shown in Fig. 8 for the baseline design and for the final design of the first optimization. The rms errors are converged to about 1.2% in the baseline case and 4.7% in the modified case. It can be deduced from Figs. 6–8 that local stress considerations require more modes than aeroelastic effectiveness and loads considerations, which are of an integrative nature. It can be also deduced that the differences between the modal and discrete values in Figs. 3–5 are mainly caused by modal stress errors.

The computations in this work were performed on a Silicon Graphics Indigo 2, R4400 workstation. A comparison between CPU time for various analysis and design modules with the discrete and modal applications of the first example is given in Table 1. In addition to the full aeroelastic analysis and optimization cases, the table shows also CPU time for aeroelastic trim and effectiveness only, and for stress under fixed loads. The first part of the table gives the CPU time for constructing the basic structural and aerodynamic matrices, which is the same for all the cases. This part is not repeated in the optimization. The second part of the table compares CPU times for analysis cases. A major difficulty in the application of the modal approach in the current version of ASTROS is its very inefficient normal mode analysis scheme. The ASTROS computation of the 45 modes took 908.1 s. The computation of the

Table 1 Comparison of CPU seconds for various analysis and optimization modules, 3761 DOF model

Module	Discrete	Modal
Global matrices	50.4	50.4
Steady aero	232.0	232.0
Analysis		
Trim and effectiveness	341.5	141.5[a]
Full aeroelastic	347.9	148.0[a]
Stress with fixed loads	69.6	140.2[a]
Database		
Trim and effectiveness	——	15.7
Full aeroelastic	——	238.5
Stress with fixed loads	——	238.1
Per iteration		
Trim and effectiveness	386.9	4.9
Full aeroelastic	395.6	23.7
Stress with fixed loads	80.8	19.8

[a]If modes calculated with Lanczos eigensolution.

same modes with MSC/NASTRAN, using the Lanczos method, took only 64.5 s. The table reflects ASTROS actual CPU times, minus the 834.6-s difference between the two eigenvalue methods. The CPU times for the two aeroelastic modal analysis cases in the table are almost 60% less than those of the discrete approach. It is, however, twice that of the discrete approach in static analysis with fixed loads (performed in separate runs with the loads computed in a previous aeroelastic analysis).

The third part of Table 1 gives the CPU time required for completing the database for the modal optimization cases. While the additional time for aeroelastic trim and effectiveness is relatively small, the time required for the calculation of the modal perturbations needed for stress considerations is much larger. The main advantage of the modal approach is the run time per iteration once the database is constructed, shown in the fourth part of Table 1. The iteration speed-up factors in this example were 80 for optimization with aeroelastic effectiveness constraints only, 17 in full aeroelastic optimization, and four for the case of static stresses with fixed loads.

The combined accuracy and efficiency considerations show that the modal approach is considerably more effective in aeroelastic trim and effectiveness cases. One can choose to perform the optimization run of this numerical example with the modal approach for calculating the loads and their derivatives, and then resort to the discrete approach for stress considerations. As can be deduced from Table 1, this would take about 150 s for analysis, an additional 16 seconds to complete the modal database, and about 86 s for each iteration. While this combination seems to be preferable in our case, the modal–perturbation approach may be more effective when many optimization trials are to be performed with the same database.

The second example is an analysis case that indicates the potential of the modal approach in multidisciplinary design with large-size models. A static aeroelastic analysis comparison was performed for an actual advanced-design internal loads model of a fighter aircraft. The model consisted of 38,328 structural elements comprising built-up fuselage, wing, and tail components. The model was reduced to 26,259 free DOFs after application of single- and multipoint constraints. The aerodynamic model was a flat panel representation of the configuration in similar nature to that of Ref. 17 and consisted of 400 elements all splined to the structure in conventional ASTROS manner. The modal–approach analysis was performed with the first 40 symmetric normal modes. Static condensation was used to alleviate the computational cost associated with calculating normal modes of large models in ASTROS.

Table 2 exhibits the timing characteristics for a steady aeroelastic 9g symmetrical pull-up condition run for discrete and

Table 2 Comparison of CPU seconds for various analysis modules, 26,259 DOF model

Module	Discrete	Modal
Preface		
Global matrices	719.1	719.1
Steady aero	9.7	9.7
Model size reduction		
MPC and SPC reductions	3740.0	3740.0
Static condensation	——	1630.4
Normal modes	——	21.5
Analysis		
Trim and effectiveness	8274.4	67.5
Total	12743.2	6188.2

modal approaches. The table is divided into three blocks. The preface block is performed once and is not repeated in subsequent design iterations. The CPU time for steady aerodynamics in this block is just for importing the coefficient matrices calculated in a previous run. The size-reduction block is repeated in each subsequent discrete design iteration, but not in modal-based iterations. The analysis block is to be repeated in each iteration in both cases. The immediate comparison to be noted is that the modal approach provided a speed-up of 122 over the discrete approach for the static aeroelastic trim and effectiveness module. This benefit is simply derived from the use of 40 modes, i.e., DOFs, for the modal approach instead of solving the full discrete problem. The largest amount of time in the size-reduction block involved matrix reduction for multipoint constraints. Additional considerable CPU time was used by the modal approach to reduce the model size before modes are calculated. The larger CPU time in model reduction for the modal approach is not an important disadvantage because this block is not repeated in modal-based design.

While detailed results of the analyses cannot be presented in this paper, a few comments are made. The accuracy, as shown and discussed in this paper and previous papers, is dependent on the number of modes as well as the derivation of modes.[12] In this case, the trimmed angle of attack was within 0.03% of the discrete value, and the pitch trim control surface was within 1.10%. All of the stability coefficient values were within 3% of the discrete values.

Optimization of structure with a model of this size is prohibitive with discrete analyses in the current computational environment. However, large benefits of multidisciplinary design optimization involve rapid derivation of internal loads models representative of structural and subsystem layouts. The results from this application indicate that the modal approach to multidisciplinary design will allow the use of large internal loads models in design optimization studies.

Conclusions

The modal-based static aeroelastic optimization scheme was reformulated and extended to deal with more analysis and design options. The new formulation facilitates a convenient integration of modal-based optimization into discrete-coordinate design schemes such as ASTROS. The method extensions include a new treatment of stresses under fixed and varying loads, and effects of mass changes on aeroelastic trim. The numerical applications to medium and large structural models demonstrated the great potential of the new scheme. The total CPU time required for modal analysis and the construction of a database for modal-based optimization was similar to that required for a single discrete analysis. Subsequent design iterations were 17–80 times faster than discrete iterations in aeroelastic cases and four times faster in stress under fixed loads cases. Analysis with a larger structure indicated even greater potential savings in multidisciplinary optimization with large-size models. Modal results were in excellent agreement with the discrete ones for all of the analyzed cases. Comparisons were also good at the end of optimization cycles with

considerable design changes. However, as the structure is being changed, the stress errors associated with the modal approach might grow beyond acceptable levels. Modal database updates may be required when design variables are changed by more than 10%. For an efficient application of the new scheme, it is important to use an efficient eigensolution method such as Lanczos.

Acknowledgments

The work of the first two authors was conducted under contract with Lockheed Martin Tactical Aircraft Systems. The work of the second author was partially supported by the Israeli Ministry of Immigrant Absorbtion. The technical support of V. B. Venkayya and U.S. Air Force Wright Laboratories/Flight Dynamics Directorate as well as Doug Neill at Universal Analytics Incorporated are gratefully acknowledged.

References

[1]Haftka, R. T., "Structural Optimization with Aeroelastic Constraints," *International Journal of Vehicle Design*, Vol. 7, Nos. 3–4, 1986, pp. 381–392.

[2]Neill, D. J., Johnson, E. H., and Confield, R., "ASTROS — A Multidisciplinary Automated Structural Design Tool," *Journal of Aircraft*, Vol. 27, No. 12, 1990, pp. 1021–1027.

[3]Climent, H., and Johnson, E. H., "Aeroelastic Optimization Using MSC/NASTRAN," *Proceedings of the International Forum on Aeroelasticity and Structural Dynamics* (Strasbourg, France), Association Aéronautique et Astronautique de France, Paris, France, 1993, pp. 1097–1116.

[4]Livne, E., Schmit, L. A., and Friedmann, P. P., "Integrated Structure/Control/Aerodynamic Synthesis of Actively Controlled Composite Wings," *Journal of Aircraft*, Vol. 30, No. 3, 1993, pp. 387–394.

[5]Bindolino, G., Lanz, M., Mantegazza, P., and Ricci, S., "Integrated Structural Optimization in the Preliminary Aircraft Design," *Proceedings of the 17th Congress of the International Council of the Aeronautical Sciences* (Stockholm, Sweden), International Council of the Aeronautical Sciences, Amsterdam, The Netherlands, 1990, pp. 1366–1378.

[6]Haftka, R. T., and Yates, E. C., Jr., "Repetitive Flutter Calculations in Structural Design," *Journal of Aircraft*, Vol. 13, No. 6, 1976, pp. 454–461.

[7]Sheena, Z., and Karpel, M., "Static Aeroelastic Analysis Using Aircraft Vibration Modes," Proceedings of the 2nd International Symposium of Aeroelasticity and Structural Dynamics (Aachen, Germany), Bonn, Germany, 1985, pp. 229–232.

[8]Karpel, M., and Sheena, Z., "Structural Optimization for Aeroelastic Control Effectiveness," *Journal of Aircraft*, Vol. 26, No. 5, 1989, pp. 493–495.

[9]Huang, X., Haftka, R. T., Grossman, B., and Mason, W. H., "Comparison of Statistical Weight Equations with Structural Optimization of a High Speed Civil Transport," *Proceedings of the AIAA/USAF/NASA/ISSMO 5th Symposium on Multidisciplinary Analysis and Optimization* (Panama City, FL), 1994, pp. 1135–1144.

[10]Karpel, M., "Multidisciplinary Optimization of Aeroservoelastic Systems Using Reduced-Size Models," *Journal of Aircraft*, Vol. 29, No. 5, 1992, pp. 939–946.

[11]Karpel, M., and Brainin, L., "Stress Considerations in Reduced-Size Aeroelastic Optimization," *AIAA Journal*, Vol. 33, No. 4, 1995, pp. 716–722.

[12]Karpel, M., and Raveh, D., "Fictitious Mass Element in Structural Dynamics," *AIAA Journal*, Vol. 34, No. 3, 1996, pp. 607–613.

[13]Karpel, M., and Presente, E., "Structural Dynamic Loads in Response to Impulsive Excitation," *Journal of Aircraft*, Vol. 32, No. 4, 1995, pp. 853–861.

[14]Karpel, M., and Wieseman, C. D., "Modal Coordinates for Aeroelastic Analysis with Large Local Structural Variations," *Journal of Aircraft*, Vol. 31, No. 2, 1994, pp. 396–403.

[15]Guyan, R., "Reduction of Stiffness and Mass Matrices," *AIAA Journal*, Vol. 3, No. 2, 1965, pp. 380–382.

[16]Johnson, E. H., and Venkayya, V. B., "Automated Structural Optimization System (ASTROS), Volume I — Theoretical Manual," Air Force Wright Aeronautical Labs., TR-88-3028, Dec. 1988.

[17]Love, M. H., Baker, D. K., and Bohlmann, J. D., "An Aircraft Design Application Using ASTROS," Air Force Wright Aeronautical Labs., TR-93-3037, June 1993.